www.czasopisma.pan.pl PAN POLSKA AKADEMIA NAUK www.journals.pan.pl

Arch. Metall. Mater. **63** (2018), 4, 1599-1607

DOI: 10.24425/amm.2018.125083

J. TIAN*, T. QU*#, D. WANG*, H. WANG*, Z. XU*, E. XINRUI*

EFFECT OF Mg AND Ca ON THE CHARACTERISTICS OF INCLUSIONS IN SULPHUR STEEL

The effects of Mg and Ca on sulfide modification of sulphur steel were studied to elucidate the difference between micro-magnesium treatment and micro-calcium treatment for the inclusion of sulphur steel. The results show that the inclusions in the steel appeared with an oxide core of Al_2O_3 and MnS wrapped. After the addition of Mg, the core was changed to spinel, and the MnS coating was changed to Mn-Mg-S. After Ca was added, the core was changed to Ca-Al-O, and the MnS coating was changed to Mn-Ca-S. The Mg content was higher than Ca content in the sulfides of the steel. Therefore, Mg was more effective than Ca in terms of sulfide modification with the same content of Mg and Ca in steel, but the yielding rate of Mg was lower than that of Ca. The Mg content in the oxide core was higher than Mg of the coating of the inclusions in the steel treated with Mg or Mg-Ca. In contrast, the Ca content in the oxide core was lower than Ca of the coating of the inclusions in the steel treated with Ca or Mg-Ca. MnS formed and precipitated during the melt solidification process. The complex sulfide (Mg-Mn-S) was precipitated around $MgO \cdot Al_2O_3$ in the Mg treated steel during the cooling process. CaS inclusion was precipitated on the $CaO \cdot Al_2O_3$ inclusions in the liquid Ca-treated steel. Thus, CaS was formed first, whereas MnS was formed during the cooling process, followed by the formation of complex sulfide (CaS+MnS), which finally precipitated around $CaO \cdot Al_2O_3$ in the Ca-treated steel.

Keywords: Mg treatment, Ca treatment, MnS, complex sulfide, inclusions

1. Introduction

Sulphur free-cutting steel was the most widely used free-cutting steel at present. To improve machinability, sulphur was added into the steel to form manganese sulfides inclusions with manganese. MnS inclusions serve as a lubricant and facilitate the breaking of the chip in the cutting process. However, MnS inclusions could easy be stretched along the rolling direction during the process of hot rolling. The elongated MnS inclusions could cause serious damage to the transverse impact toughness of the steel, which leads to anisotropic properties. Therefore, modification of the manganese sulfide is necessary to eliminate or reduce the negative influence of MnS on the mechanical properties of steel, and to improve the cutting performance of the steel. At present, Ca and Mg were used separately to modify sulfides in steel both at home and abroad.

Mg had exceedingly strong thermodynamic affinities with oxygen and sulphur, and magnesia inclusions have poorer agglomeration properties than alumina inclusions [1-3]. Zhang et al. [4,5] studied the effect of Mg on the evolution of sulfide in liquid steel, and found that Mg deoxidation products of low-S content experimental steel were changed in the following order $Al_2O_3 \rightarrow MgAl_2O_4 \rightarrow Mg-Al-O-S \rightarrow Mg-O-S$. On the other hand, high-S content experimental steel generated Mg – S(–O) + MnS complex inclusions. Fu et al. [6] investigated the inclusion characteristics of 35CrNi3MoV steel treated with Mg. They found that the MnS inclusions in the steel were replaced by small $MgO \cdot MgS$ or $MgO \cdot MgS \cdot MnS$ complex inclusions after addition of Mg.

A number of related studies on the influence of Ca treatment on MnS inclusions in the steel had been reported. Previous studies showed that Ca treatment promote the nucleation of sulfides on calcium aluminate complex inclusions, and Ca combined with MnS to form MnS-CaS complex sulfide. [7-10] This type of complex sulfides reduced the relative plasticity and hot deformability of sulfides during the hot rolling process. Hilty and Farrel [11] obtained the same result, indicating that: the calcium additions to manganese sulfide altered the deformation characteristics of the latter significantly, affecting the behavior of steels with MnS inclusions. The solubility of calcium in the MnS inclusion and its effect on the hardness of the latter were first examined by Chao. [12] The presence of 1% of Ca increased the diamond pyramid hardness by approximately 25% at 25°C. Research found that the addition of Ca or Mg to the steels could improve the transverse Charpy impact value without changing the longitudinal Charpy impact value because the addition of Ca or Mg to the steel led to the production of sulfides, (Mn, Ca)S or (Mn, Mg)S, respectively, and the elongation of these complex sulfides during hot forging were more difficult than that of MnS inclusions.

* SOOCHOW UNIVERSITY, SHAGANG SCHOOL OF IRON AND STEEL, SUZHOU 215021, PR CHINA

Corresponding author: jtian@suda.edu.cn

In the current study, the experimental steels were treated by Mg, Ca, and Ca-Mg respectively. The composition, size, morphology, and formation mechanism of inclusions were investigated based on the experiment and thermodynamic calculation. This study aiming at revealing the different effects of Mg and Ca on sulfide modification of steel, and it would be helpful to improve the effect of calcium treatment and Mg treatment.

2. Experimental

The experiment was carried out by using a vertical resistance furnace as shown in Fig. 1. First, approximately 400 g pure iron was put into a magnesia crucible (70 mm in diameter and 120 mm in height), which was then transferred into the graphite crucible (protection) putted in the furnace under argon atmosphere at a flow rate of 2.0 $L \cdot min^{-1}$. When the temperature was raised to 1873 K, the molten iron was held for 10 min. Further, the dissolved oxygen of the melt was measured by an oxygen-content probe. Based on the level of dissolved oxygen, pure Al wire was added into the molten steel. After 2 min, the ferromanganese and sulphur powder were put into the melt, followed by immediate stirring for 10 s using a molybdenum stick. After 5 min, sample 1# was extracted by a quartz tube (8 mm in diameter) from the melt, and immediately quenched in cold water. Next, Ni-Mg alloy(80 mass % Mg) was added into the melt, which was stirred for 10 s using the molybdenum stick. Then, the dissolved oxygen was subsequently measured in the same way as described before. Thereafter, the melt was held for 1, 5, 10 and 15 min respectively and was sampled by a quartz tube, followed by rapid quenching (sample 2#, 3#, 4#, and 5#, respectively).

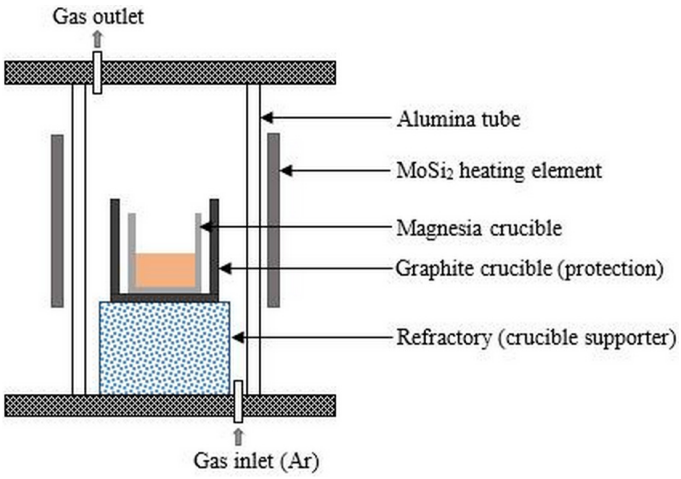

Fig. 1. Schematic diagram of the vertical resistance furnace

The experimental procedures of Ca and Ca-Mg treatment were identical to the procedure of Mg treatment experiment, mentioned above. The difference was that the Ni-Mg alloy was replaced with pure Ca granules and Mg-Ca alloy (80 mass % Mg), respectively, during the procedure of Ca and Ca-Mg treatments experiment.

After the completion of all experiments, the contents of C, S of the steel samples were analyzed using infrared analyzed. The concentrations of Mn, Mg, Ca, Als(dissolved aluminum) and T.O(dissolved oxygen) were determined using ICP-OES (inductively coupled plasma-atomic emission spectroscopy), and the results were shown in Table 1. All the samples were cross-sectioned and polished, and then morphology and composition of inclusions were analyzed by SEM (Scanning Electron Microscopy) and EDS (Energy Dispersive Spectrometer).

TABLE 1

Chemical composition of experimental steels (wt%)

No.	C	Mn	S	Als	T.O	Mg	Ca
A	0.14	1.02	0.039	0.120	0.0020	0.0007	—
B	0.17	1.02	0.040	0.066	0.0026	—	0.0009
C	0.13	1.02	0.039	0.110	0.0028	0.0008	0.0008

3. Results and discussion

3.1. Morphology and composition of the inclusions

The morphology and composition of typical inclusions of the samples determined in Fig. 2. As can be seen from the figure, the inclusions had a two-layer complex structure, consisting of an oxide core surrounded by sulfide. In the steel without treatment with Mg, Ca, or Mg-Ca, the cores contained Al_2O_3 inclusions, and the coating of Al_2O_3 inclusions were MnS, as shown in Fig. 2(A-1), (B-1), and (C-1). The oxide cores were comprised of magnesia-alumina spinel surrounded by composite sulfide Mn-Mg-S in the Mg-steel, as shown in Fig. 2(A-2) ~ (A-5). In the Ca-treated steel, the oxide cores were made of Al-Ca-O inclusions which ware surrounded by Mn-Ca-S composite sulfides as displayed in Fig. 2(B-2) ~ (B-5). The oxide cores of the steel treated with Mg-Ca alloy were composed of Mg-Ca-Al-O inclusions surrounded by Mn-Ca-Mg-S composite sulfide.

From Fig. 2, it can be observed that the oxide cores of the steel treated with Mg or Mg-Ca alloy were irregular, and the profiles of the former were distinct, whereas those of the latter were indistinct and close to spherical. The oxide cores of the Ca-treated steel were spherical.

The Ca and Mg content at different positions (oxide core and sulfide coating) of the inclusions in different samples were plotted against the holding time after the Mg treatment (melt No. A), Ca treatment (melt No. B) and Mg-Ca treatment (melt No. C), as shown in Fig. 3. The Mg content in the oxide core was higher than that in the coating, Fig. 3(A) and (C). In contrast, the Ca content in the oxide was lower than that in the coating, Fig. 3(B) and (C). Moreover, the Mg content of the sulfide was higher than its Ca content in the steel with the same content of Mg and Ca as show in Fig. 3. The higher Mg or Ca content of the MnS, increased the hot hardness of the sulfide [13]. These complex sulfides containing Mg or Ca were more difficult than

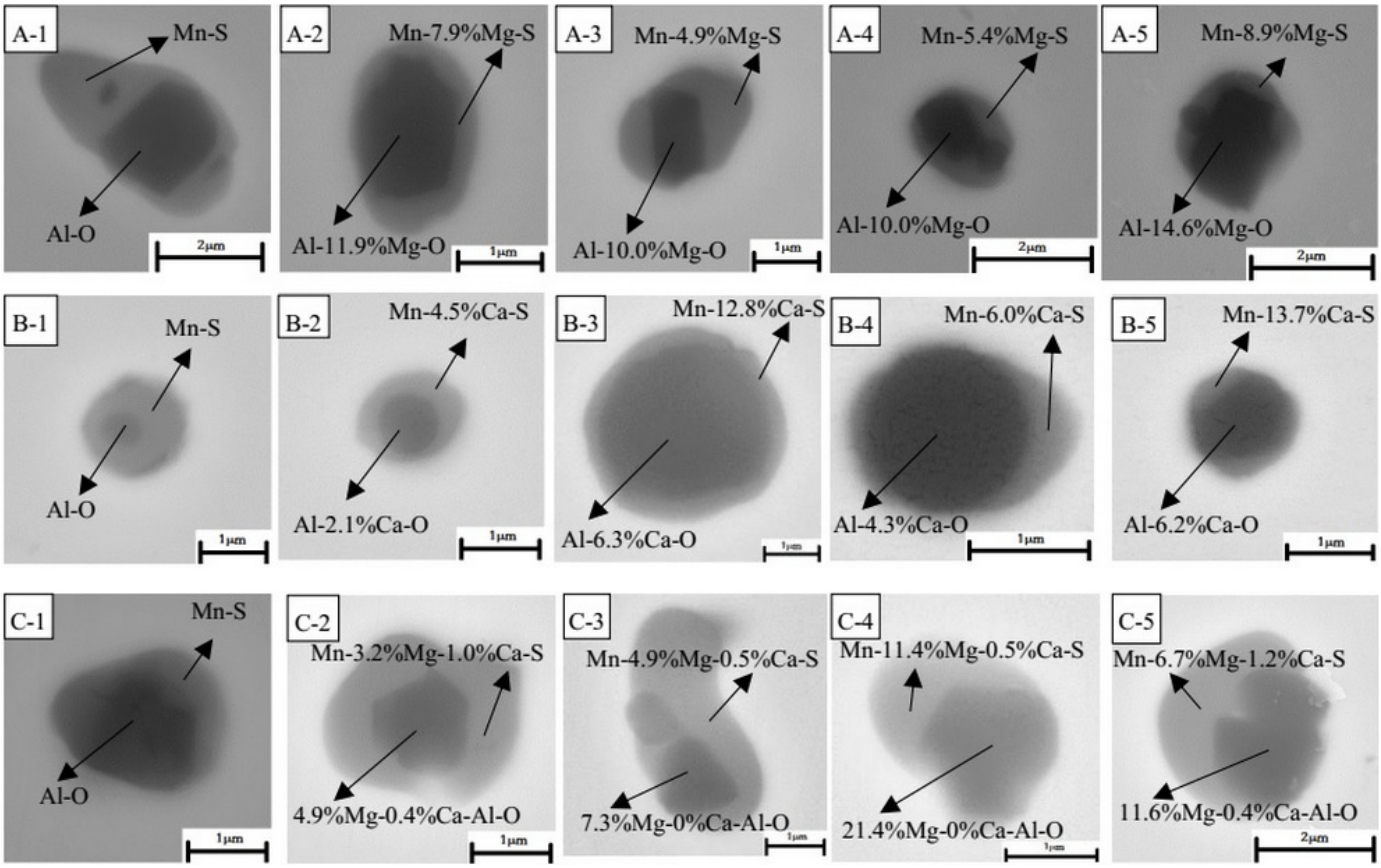

Fig. 2. Morphology and composition of typical inclusions of the samples. A, B, and C indicate melt numbers; 1, 2, 3, 4, and 5 denote samples 1#, 2#, 3#, 4#, and 5#, respectively

pure MnS inclusions to elongate during hot forging, which affects positively the transverse impact toughness of steel. Therefore, Mg is more effective than Ca in terms of sulfide modification with the same content of Mg and Ca in steel, but the yielding rate of Mg is lower than that of Ca.

3.2. Evolution mechanism of inclusion

3.2.1. Effect of Ca and Mg on the oxide core

The morphology of the oxide core was irregular in the samples of melt No.A after the Mg treatment, shown in Fig. 2(A-2) ~ (A-5). The following reactions occurred in melt No. A after Mg treatment:

$$2[Al] + 3[O] = Al_2O_3(s)$$
$$\Delta G^0 = 867500 - 222.5T \text{ [14]} \quad (1)$$

$$[Mg] + [O] = MgO(s)$$
$$\Delta G^0 = 90000 - 82.0T \text{ [14]} \quad (2)$$

After addition of Mg, the formation of $MgO \cdot Al_2O_3$ can be summarized as follows:

$$Al_2O_3(s) + [Mg] + [O] = MgO \cdot Al_2O_3(s)$$
$$\Delta G^0 = -110720 - 93.51T \text{ [15]} \quad (3)$$

$$MgO(s) + 2[Al] + 3[O] = MgO \cdot Al_2O_3(s)$$
$$\Delta G^0 = -887960 + 210.88T \text{ [15]} \quad (4)$$

$$[Mg] + 2[Al] + 4[O] = MgO \cdot Al_2O_3(s)$$
$$\Delta G^0 = 978182 - 128.93T \text{ [4]} \quad (5)$$

$$MgO(s) + Al_2O_3(s) = MgO \cdot Al_2O_3(s)$$
$$\Delta G^0 = -20740 - 11.57T \text{ [15]} \quad (6)$$

The stability diagram of MgO, $MgO \cdot Al_2O_3$ and Al_2O_3 at 1873K was calculated as a function of mass percent of Mg and Al by software FactSage 7.0 based on Eqs. (3) through (5), presented in Fig .4. The melt was assumed to be an ideal solution, and a dilute solution of 1mass% standard solution was used in the present study. The activities of the element can be calculated using Eqs. (7) and Wagner's equation (Eqs. (3)) according to the chemical composition (Table 1) and thermodynamic data, listed in Table 2 [16].

$$a_i = f_i \times [\%i] \quad (7)$$

$$\log f_i = \sum_{j=2}^{n} e_i^j [\%j] + \sum_{j=2}^{n} r_i^j [\%j]^2 + \sum_{j=2}^{n-1} \sum_{k=3}^{n} r_i^{j,k} [\%i][\%k] \quad (8)$$

As can be seen in Fig. 4, the composition point of melt No. A and melt No. C were located in the $MgO \cdot Al_2O_3 + Al_2O_3$ region. Thus, the oxide cores in melt No. A were irregular after the addition of Mg, as shown in Fig. 2(A-2) ~ (A-5).

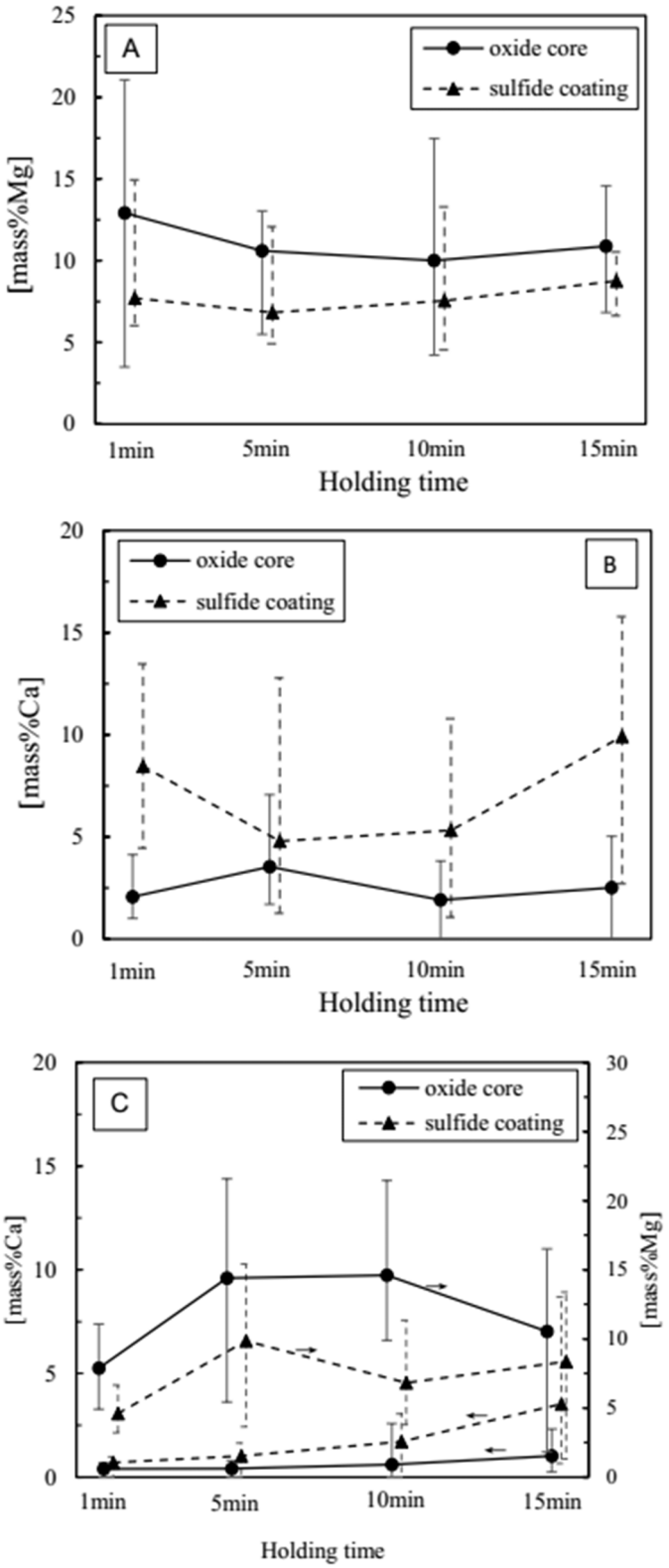

Fig. 3. Effect of the holding time on Ca and Mg content at different position of inclusions

TABLE 2

Interaction parameters of elements in liquid iron at 1,873 K

i	j	k	e_i^j	r_i^j	$r_i^{(j,k)}$
Al	Mg	Al	–0.13 [17]	0 [18]	0 [18]
		O			–260 [18]
	O	Al	–1.98 [17]	39.82 [19]	–0.028 [19]
		Mg			–260 [20]
	S	—	0.03 [21]	—	—
	Al	O	0.043 [17]	–0.001 [22]	–0.028 [19]
		Mg			0 [18]
	Ca	—	–0.047 [23]	—	—
	Mn	—	0.035 [24]	—	—
O	Mg	O	–280 [25]	–20,000 [15]	462,000 [15]
		Al			–150 [18]
	O	—	–0.17 [17]	—	—
	S	—	–0.133[24]	—	—
	Al	O	–1.17 [17]	–0.010 [19]	47 [15]
		Ca			0 [15]
	Ca	O	–310 [15]	–18,000 [15]	520,000 [15]
		Mg			0 [15]
	Mn	—	–0.021 [26]	—	—
S	Al	—	0.035 [21]	0.0009 [27]	—
	Mg	—	–0.026 [27]	—	—
	O	—	–0.027 [23]	—	—
	S	—	–0.028 [21]	–0.0009[27]	—
	Ca	—	–110 [23]	—	—
	Mn	—	–0.026 [26]	—	—
Mn	Mg	—	—	—	—
	O	—	–0.083 [26]	—	—
	S	—	–0.048 [24]	—	—
	Al	—	0.027 [24]	—	—
	Ca	—	–0.023 [27]	—	—
	Mn	—	0.024 [28]	—	—
Mg	Mg	O	–0.047 [15]	—	48,000 [15]
	O	Al	–430 [25]	350,000 [15]	–230 [20]
		Mg			61,000 [15]
	S	—	—	—	—
	Al	O	–0.27 [28]	—	–230 [15]
	Ca	—	—	—	—
	Mn	—	—	—	—
Ca	Mg	—	—	—	—
	O	—	–780 [28]	650,000 [15]	—
	S	—	–132 [29]	—	—
	Al	—	–0.072 [23]	0.0007 [28]	—
	Ca	O	–0.002 [23]	—	90,000 [15]
	Mn	—	–0.0156 [26]	—	—

The steel was treated with Ca, whose oxide cores were composed of calcium-aluminates, as displayed in Fig. 2B. The calculation of the reactions was conducted based on Eq. (9) [30]. The activities of CaO and Al_2O_3 in different calcium aluminates were listed in Table 3. The standard state was infinitude dilute solution in liquid steel. And the first order, second order interaction parameters and cross product terms were considered during the calculation. The thermodynamic calculation result was shown in Fig. 5. It shown that the equilibrium content of aluminum and calcium equilibrated with different calcium aluminates in liquid steel at 1873K. The oxide inclusions of the samples of melt No. B after treatment with calcium were in the region of $CaO \cdot Al_2O_3$ (The asterisk in the figure denoted the composition

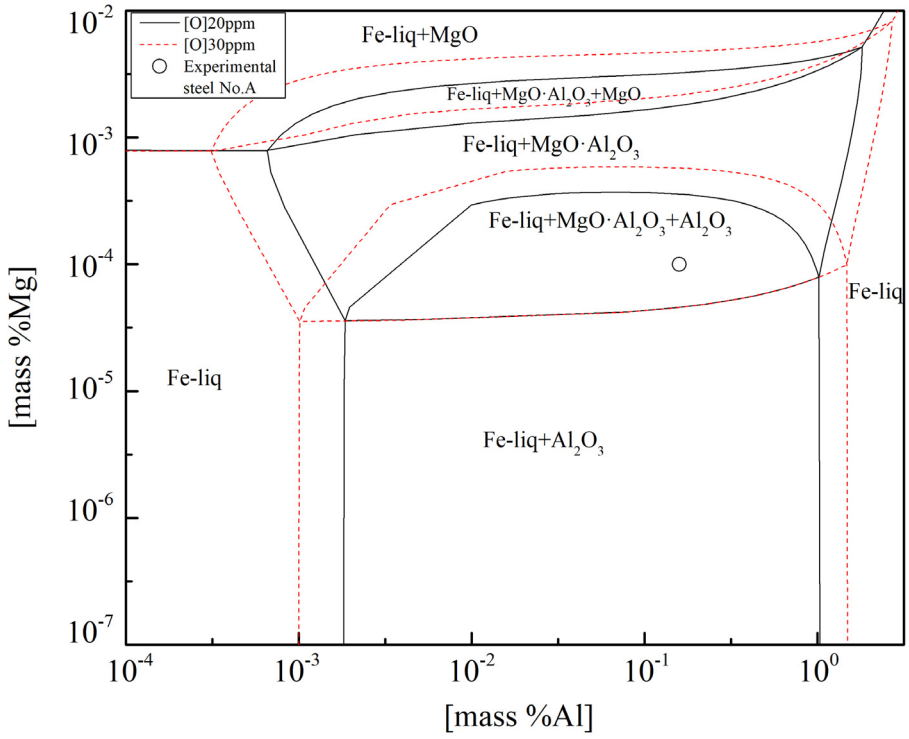

Fig. 4. Stability diagram of MgO, $MgO \cdot Al_2O_3$, and Al_2O_3 inclusions with different oxygen content (20 ppm and 30 ppm) at 1,873 K

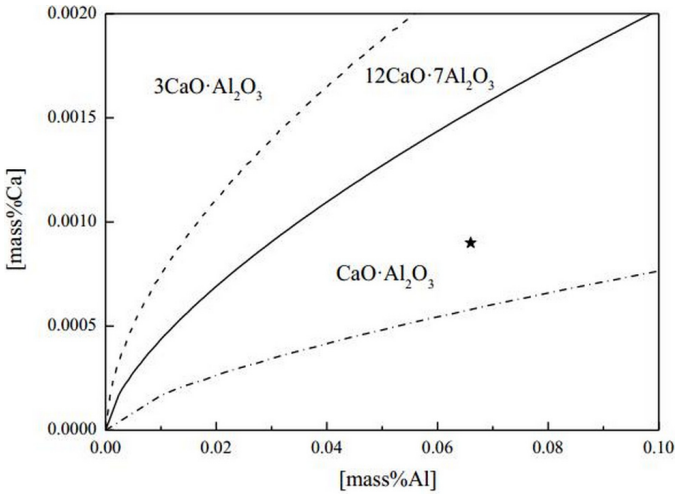

Fig. 5. Phase stability diagram of the Al-Ca-O in molten steel at 1,873 K

of the steel), according to the composition, listed in Table 1. The $CaO \cdot Al_2O_3$ was liquid in the steel at steel making temperature, so, the oxide cores of the Ca-treated steel were spherical as shown in Figs. 2(B-2) ~ (B-5).

$$2[Ca] + (Al_2O_3)incl = 2[Al] + 3(CaO)incl$$
$$\log K = 5667/T - 2.58 \text{ [31]} \quad (9)$$

The morphology of oxide core in melt C was close to spherical, as shown in Fig. 2(C-2) ~ C-5). The composition of the inclusions in the steel at different time points after the Ca treatment could be observed in Fig. 6, the region of the black circle was the liquid region at the bottom of the ternary phase diagram. As shown in the figure, all inclusions were beyond the

TABLE 3

Activities of CaO and Al_2O_3 in different calcium aluminates at 1,873 K [31,32]

Calcium aluminates	a_{CaO}	a_{Al2O3}	Melting point (K)
$3CaO \cdot Al_2O_3$	0.773	0.010	1,808
$12CaO \cdot 7Al_2O_3$	0.340	0.064	1,728
$CaO \cdot Al_2O_3$	0.340	0.275	1,878

liquid region, and thus shapes of the oxide cores were irregular (triangle, rectangular, or square). Enlarge the region of the ellipse region in the ternary phase diagram, as shown in the figure 6 on the left, and it could be shown that the inclusions have more content of CaO as time goes on after Ca-Mg treatment. The average content of Ca at different positions (oxide core and sulfide coating) of inclusions of different samples was exhibited in Fig. 3(C). The error bars represent the ranges of minimum and maximum values. As can be seen from the figure, Ca content of the coating was higher than that of the cores. This transition process of the oxide core was described by the schematic in Fig. 7. Initially, there was a little Ca content (C_0) in the oxide core, the Ca content of the outside coating was C_1 ($C_1 > C_0$), as shown in Figure 7 (on the left). Then, with time, Ca diffuses into the oxide core from the outside sulfide coating because of the concentration gradient. The content of Ca in the outside edge of the oxide core may reach C'_0 (Figure 7, on the right). Therefore, some outside edge of the oxide core likely contains sufficient CaO leading to the composition of these outside edges reaching the liquid region. In other words, some parts of the outside edge of the inclusions were liquid at 1873K, and thus, these shapes of inclusions were close to spherical.

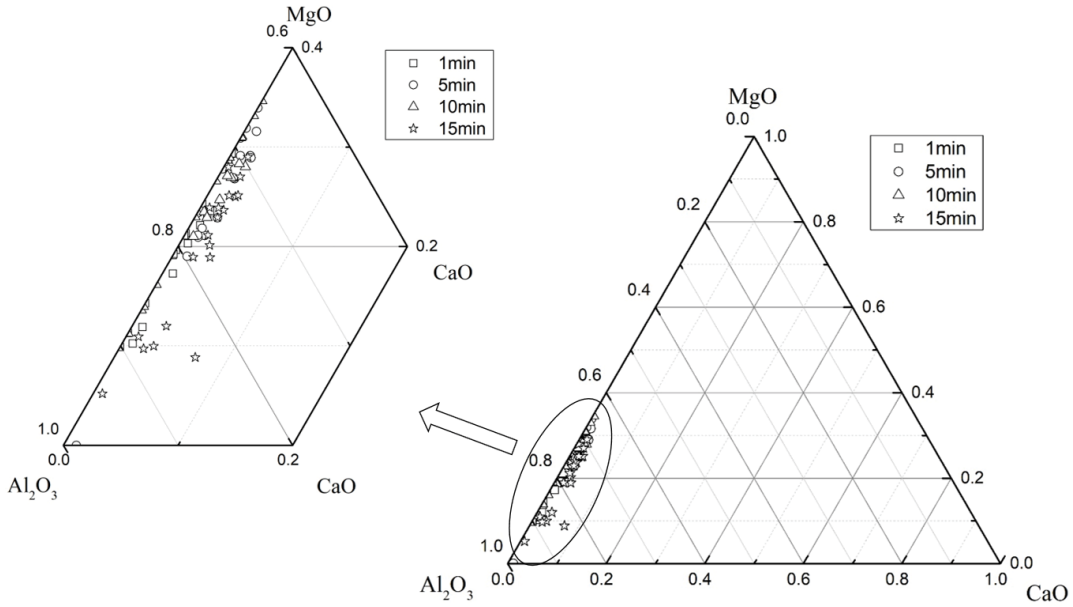

Fig. 6. Composition of the inclusions in the steel with the Mg-Ca treatment

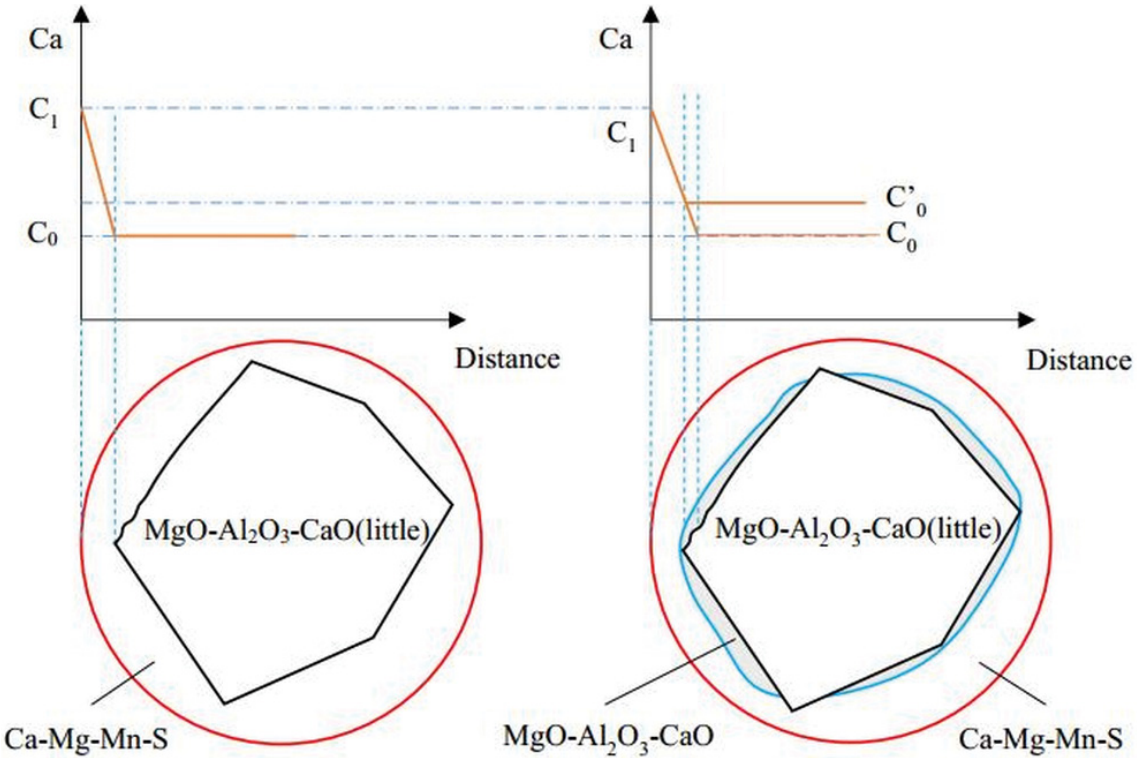

Fig. 7. Schematic diagram of the transition process of the oxide core in Mg-Ca-treated steel

3.2. Effect of Ca and Mg on MnS inclusion

The following reactions took place in the molten steel after Mg or Ca treatment.

$$[Mg] + [S] = MgS(s)$$
$$\Delta G^0 = -539740 + 193.05T \text{ [4]} \quad (10)$$

$$[Ca] + [S] = CaS(s)$$
$$\Delta G^0 = -530900 + 116.20T \text{ [33]} \quad (11)$$

$$[Mn] + [S] = MnS(s)$$
$$\Delta G^0 = -167612 + 88.70T \text{ [34]} \quad (12)$$

The critical temperature for MgS, CaS and MnS formation could be calculated by Eqs. (10-12). The liquidus temperature (T_{Liq}) and solidus temperature (T_{Sol}) of the steel were calculated by the following formulas [35], all calculated results were presented in Table 4. From the table, the critical formation temperature of MnS was lower than the experimental temperature (1873K), thus, MnS could not be formed in the experimental

steel at 1873K. The critical formation temperature of MgS and CaS were higher than 1873K, so, both of them will be produced at the experimental temperature.

$$T_{Liq}(°C) = 1536 - 83[\%C] - 7.8[\%Si] - 5[\%Mn + \%Cu] - 32[\%P] - 31.5[\%S] - 3.6[\%Al] - 1.5[\%Cr] - 2[\%Mo] - 4[\%Ni] - 18[\%Ti] - 2[\%V] \quad (13)$$

$$T_{Sol}(°C) = 1536 - 334[\%C] - 12.3[\%Si] - 6.8[\%Mn] - 124.5[\%P] - 183.5[\%S] - 4.1[\%Al] - 1.4[\%Cr] - 4.3[\%Ni] \quad (14)$$

TABLE 4

Critical sulphide formation temperature and liquidus and solidus temperatures of the melt

No.	Critical formation temperature /K			Liquidus temperature /K	Solidus temperature /K
	CaS	MgS	MnS		
A	—	1,954.70	1,335.87	1,790.66	1,746.30
B	2,146.35	—	1,404.73	1,788.29	1,735.97
C	2,263.48	2,104.57	1,405.32	1,791.68	1,749.74

As it is evident from the table, the critical temperature of MnS formation was lower than the solidus temperature. Therefore, it could be inferred that MnS inclusions were formed and precipitated during the solidification process of the melt. The MgS and CaS inclusions were formed at the experimental temperature without considering the effect of oxygen in the melt.

Eq. (15) obtained by using a linear combination based on Eqs. (1), (2), (6) and (10). Fig. 8 displayed the relationship between Al and S in the molten steel as calculated by Eq. 14. The activities of MgO, $MgO \cdot Al_2O_3$, and MgS were assumed as unity, and the activities of Al and S were calculated by Eqs. (7,8). The composition plots of the experimental steel (No. A and No. C) were plotted in Fig. 8.

$$2[Al] + 3[S] + 4MgO = MgO \cdot Al_2O_3 + 3MgS$$
$$\Delta G^0 = -2184422 + 1060T \quad (15)$$

It is obvious that MgS could not be formed at 1873K but was formed in the experimental melt at the temperature of over 1773K. Therefore, under the experimental conditions of the present study, MgS was precipitated during the solidification of the melt.

Based on the experimental observations made and the thermodynamic analysis conducted, the formation of complex sulfide in the Mg-treated steel could be summarized by the steps displayed in the schematic in Figure 10.

Firstly, Mg reacted with Al_2O_3 to form $MgO \cdot\cdot Al_2O_3$ according to Eq. (3). Subsequently, the dissolved Mg and Mn react with the dissolved sulphur to form MgS + MnS, and the complex sulfide was precipitated around $MgO \cdot\cdot Al_2O_3$ during cooling process. Initially, most of Mg in the molten steel was consumed during the formation of $MgO \cdot Al_2O_3$, and thus, the Mg level in the oxide core was higher than that in the outside coating, as shown in Fig. 3(A) and (C).

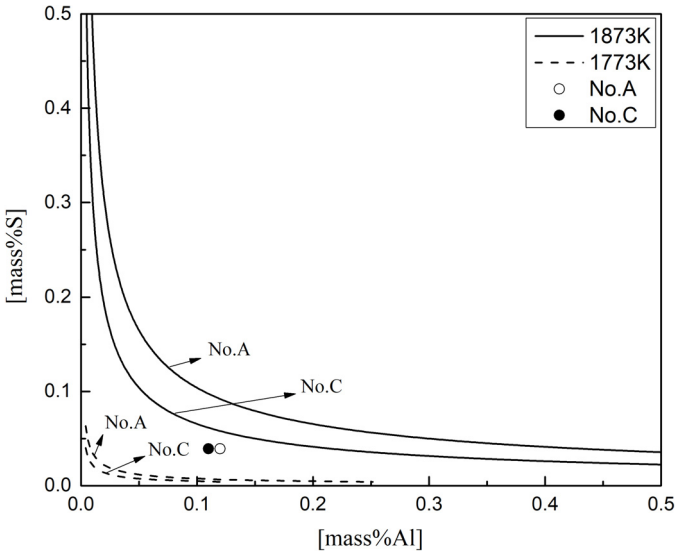

Fig. 8. Equilibrium phase diagram of MgS-$MgO \cdot Al_2O_3$ reaction at 1,873K. and 1,773K

Figure 9 represented the relationship between Al and S in the melt as calculated by the following equation (16) with the activities of CaO and Al_2O_3 in different calcium aluminate phases The vaule of the activity of CaS was taken as 0.75 as there was a transient CaS mixed with transient MnS [36]. The composition plots of experimental steel (No.B and No.C) were exhibited in this figure. It could be seen that the composition of calcium aluminate in both steels were in the region of $CaO \cdot Al_2O_3$ according to the concentration of sulfur and aluminum in the molten steel. That is, calcium aluminate phases were $CaO \cdot Al_2O_3$ in both steel. Under the premise that the calcium aluminate in the composite inclusions was $CaO \cdot Al_2O_3$, as shown in Fig. 5, the CaS could be precipitated on the $CaO \cdot Al_2O_3$ inclusions in the liquid steel.

$$2[Al] + 3[S] + 3(CaO)_{incl} = (Al_2O_3)_{incl} + 3(CaS)_{incl}$$
$$\log K = 44273/T - 15.12 \text{ [31]} \quad (16)$$

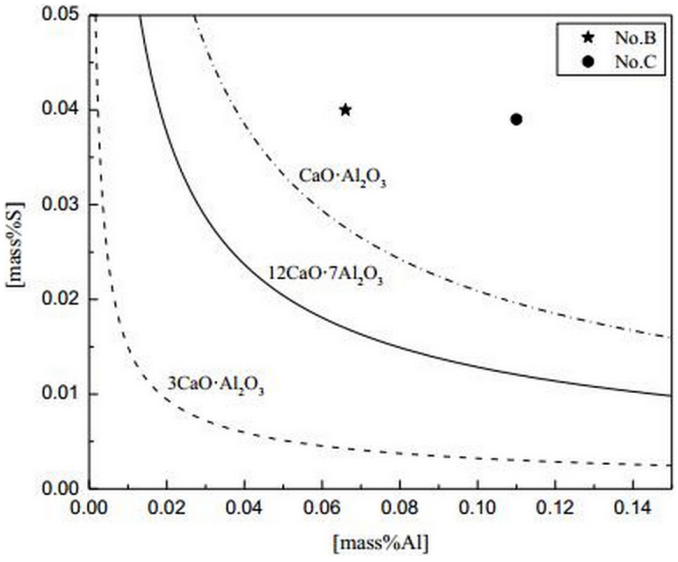

Fig. 9. Relationship between Al and S in the melt at 1,873K

Figure 10 displayed the schematic of the formation of complex sulfide in the calcium treated steel. Calcium reacted with Al_2O_3 and S to form calcium aluminum and CaS according to Eqs. (9) and (11). Then, CaS could be precipitated on the surface of calcium aluminum at the steelmaking temperature and during the solidification. Therefore, the calcium content in the oxide core was lower than that in the outside coating, as presented in Fig. 3(B) and (C). Importantly, MnS could be precipitated during the cooling process only.

According to the research finding discussed above, the formation of complex sulfide in the steel treated by Mg-Ca alloy could be performed by following the processed illustrated in Figure 10.

4. Conclusions

In the current study, we performed laboratory experiments and thermodynamic calculation to elucidate the mechanisms formation and modification of the oxide cores and sulfide in the experimental steel treaded by Mg, Ca, and Ca-Mg alloy, respectively. Based on the results obtained, the following major conclusions were could be drawn:

(1) The inclusions in steel appear with an oxide core of Al_2O_3 and MnS wrapped. The core was changed to spinel after treatment with Mg in the steel, and the MnS coating was changed to MnS + MgS. The steel treated with Ca obtained an identical structure, the core was changed to $CaO + Al_2O_3$ after the treatment, and the MnS coating was changed to MnS + CaS.

(2) The Mg content was higher than Ca content in the sulfides of the steel. Therefore, Mg was more effective than Ca in terms of sulfide modification with the same content of Mg and Ca in steel, but the yielding rate of Mg was lower than that of Ca.

(3) The Mg content in the oxide core was higher than that in the coating of the inclusions in the steel treated with Mg or Mg-Ca. In contrast, the Ca content in the oxide was lower than that in the coating core of the inclusions in the steel treated with Ca or Mg-Ca.

(4) Based on the thermodynamic calculation, the MnS inclusion was formed and precipitated during solidification process of the melt. MgS inclusion could not be formed at 1873K but was formed in the experimental melt at a temperature of over 1773K. Therefore, MgS was precipitated during the solidification of the melt under the experimental conditions employed in the present work. Then, the complex sulfide (MgS + MnS) was precipitated around $MgO \cdot Al_2O_3$ during the cooling process in the Mg-treated steel. The inclusion of CaS was precipitated on the $CaO \cdot Al_2O_3$ inclusions in

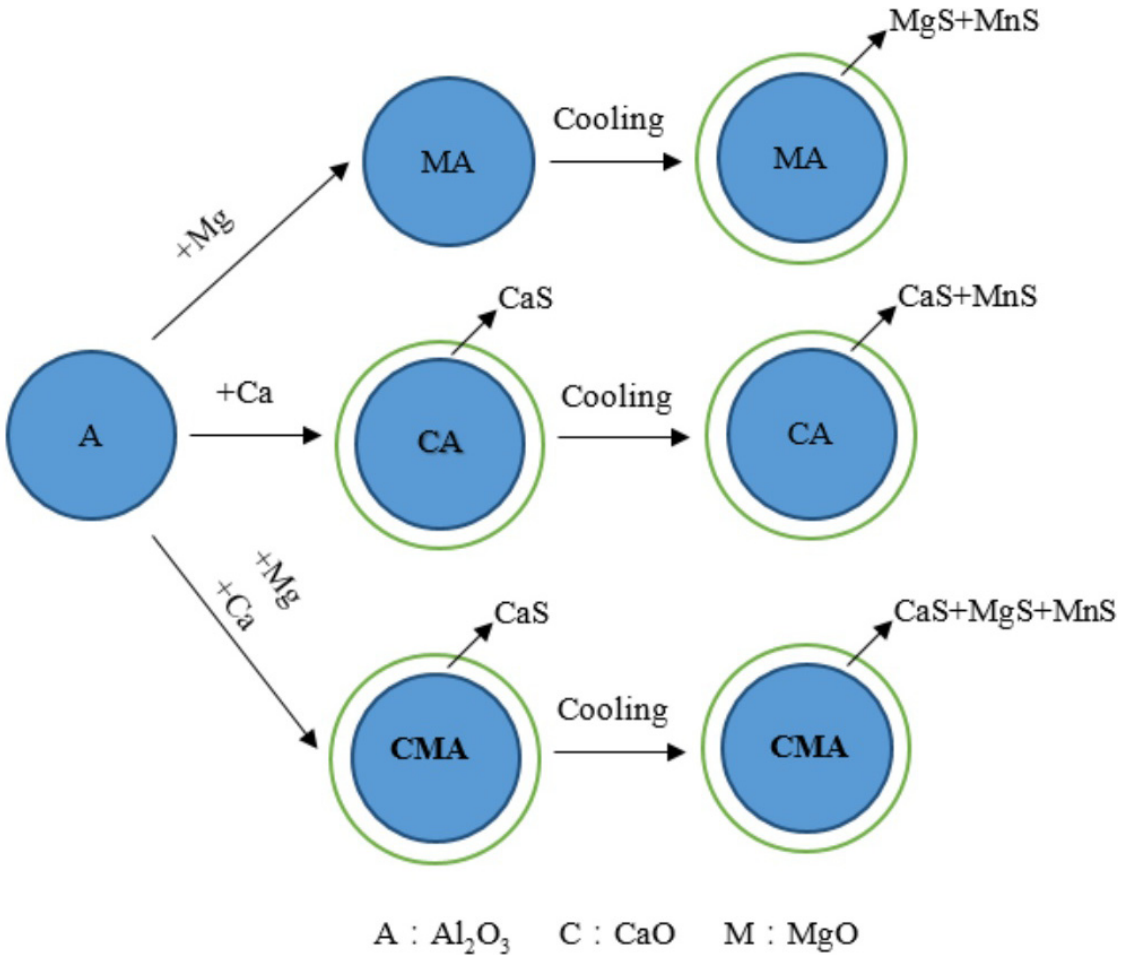

Fig. 10. Schematic diagram of the formation of complex sulfide in the steel treated by Ca, Mg and Ca-Mg, respectively

the liquid Ca-treated steel. Therefore, CaS was formed first, whereas, MnS was generated during the cooling process. Finally, the complex sulfide (CaS + MnS) was precipitated around $CaO \cdot Al_2O_3$ in the Ca-treated steel.

Acknowledgments

The authors wish to express their application to the National Natural Science Foundation of China (No. 51704200, No. 51674172) and Jiangsu province Natural Science Fund (BK20150336, BK20150334) for providing financial support which enabled this study to be carried out.

REFERENCES

[1] R. Takata, J. Yang, M. Kuwabara, ISIJ Int. **47** (10), 1379-1386 (2007).
[2] H. Ohta, H. Suito, ISIJ Int. **46** (1), 42-49 (2006).
[3] Z.H. Jiang, Y. Zhuang, Y. Li, J. Iron. Steel. Res. Int. **20** (5), 6-10 (2013).
[4] T.S. Zhang, D.Y. Wang, M. F. Jiang, **21** (12), 1073-80 (2014).
[5] T.S. Zhang, D.Y. Wang, C.W. Liu, J. Iron. Steel. Res. Int. **21** (Suppl.), 99-103 (2014).
[6] J. Fu, Y.G. Yu, A R. Wang, J. Mater. Sci. Technol. **14** (1), 53-56 (1998).
[7] T.M. Banks, T. Gladman, Met. Technol. **6** (3), 81-94 (1979).
[8] Y. Kusano, Y. Kawauchi, M. Wajima, ISIJ Int. **36** (Suppl.), 77-80 (1996).
[9] G.Z. Li, F.M. Wang, R. Hui, Int. J. Min. Met. Mater. **16** (6), 650-653 (2009).
[10] B. Carl, L. Gilles, L. Hoang, Mater. Charact. **38** (1), 25-37 (1997).
[11] D.C. Hilty, J.W. Farrell, Cim. Bull. **67** (748), 47 (1974).
[12] H.C. Chao, L.H. Van Vlack, F. Oberin, L. Thomassen, ASM Trans. Q. **57** (4), 885-891 (1964).
[13] C.H. Leung, L.H. Van Vlack, Metall. Trans. A. **12** (6), 987-991 (1981).
[14] H. Itoh, M. Hino, S. Ban-ya, Tetsu-To-Hagane. **83**, 773-778 (1997).
[15] H. Itoh, M. Hino, S. Ban-Ya, Metall. Mater. Trans. B. **28** (5), 953-956 (1997).
[16] T.S. Zhang, D.Y. Wang, C.W. Liu, J. Iron. Steel. Res. Int. **21** (Suppl.), 99-103 (2014).
[17] T. Nishi, K. Shinme, Tetsu-to-Hagane. **84** (12), 837-843 (1998).
[18] N. Satoh, T. Taniguchi, S. Mishima, Tetsu-to-Hagane. **95** (12), 827-836 (2009).
[19] H. Itoh, M. Hino, B.Y. Shiro, Tetsu-to-Hagane. **83** (12), 773-778 (1997).
[20] H. Itoh, M. Hino, S. Ban-Ya, Tetsu-to-Hagane. **84** (2), 85-90 (1998).
[21] S.W. Cho, H. Suito, **34** (2), 177-185 (1994).
[22] F. Ishii, B.Y. Shiro, M. Hino, **36** (1), 25-31 (1996).
[23] Y. Higuchi, M. Numata, S. Fukagawa, Tetsu-to-Hagane, **82** (8), 671-676 (1996).
[24] Z. Ma, D. Janke, ISIJ Int. **38** (1), 46-52 (1998).
[25] H. Itoh, M. Hino, S. Banya, Tetsu-to-Hagane. **83** (10), 623-628 (1997).
[26] H. Suito, R. Inoue, ISIJ Int. **36** (5), 528-536 (1996).
[27] H. Ohta, H. Suito, ISIJ Int. **36** (8), 983-990 (1996).
[28] J.H. Park, S.B. Lee, Mater. Trans. B. **39** (6), 853-861 (2008).
[29] K. Taguchi, O.N. Hideki, D. Nakai, ISIJ Int. **43** (11), 1705-1709 (2003).
[30] H. Mitsutaka, I. Kimihisa, Tohoku University Press: Thermodynamic Data for Steelmaking, Sendai (2010).
[31] S. Ueda, O.N. Hideki, Bulletin of the Iron & Steel Institute of Japan. **11** (4), 208-214 (2006).
[32] B. Korousic, Steel Res. **62** (7), 285-288 (1991).
[33] H. Suito, R. Inoue, ISIJ Int. **36** (5), 528-536 (1996).
[34] J. Fu, Y. Yu, A. Wang, J. Mater. Sci. Technol. **14** (1), 53-56 (1998).
[35] R. Diederichs, W. Bleck, Steel. Res. Int. **77** (3), 202-209 (2006).
[36] D.Z. Lu, G.A. Irons, W.K. Lu, Ironmak Steelmak. **18** (5), 342-346 (1991).